Study of Reflection-Loss-Based Material Identification from Common Building Surfaces

Yi Geng
Ericsson R&D
Nanjing, China
yi.a.geng@ericsson.com

Vijaya Yajnanarayana
Ericsson Research
Banglore, India
vijaya.yajnanarayana@ericsson.com

Ali Behravan
Ericsson Research
Kista, Sweden
ali.behravan@ericsson.com

Erik Dahlman
Ericsson Research
Kista, Sweden
erik.dahlman@ericsson.com

Deep Shrestha
Ericsson Research
Linköping, Sweden
deep.shrestha@ericsson.com

***Abstract*—Perceiving and recognizing material properties of surfaces and objects are fundamental aspects of new and emerging use cases such as robotic perception, virtual reality (VR) applications, digital twins, and creating a 3D digital map of an environment. In this paper, we present results from our simulation-based study of reflection-loss-based material identification from eight common building materials. The study focuses on 2.6 GHz, 28 GHz, and 60 GHz radio carrier frequencies. Analysis of simulation results indicates that a combination of incident angle and reflection loss can be used to properly identify the common building materials. We, therefore, propose a novel joint communication and sensing method for material recognition using reflection loss of the radio signal by the scatterers around the propagation path in a wireless communication network. Compared to existing material identification methods, the proposed reflection-loss-based method is capable of identifying materials from a significant distance without requiring any contact with the object and without requiring dedicated sensors from the infrastructure point of view.**

***Index Terms*—material identification, reflection loss, path loss, incident angle, joint communication and sensing**

I. Introduction

Material recognition is the process of identifying material of an object and is a fundamental aspect of many new and emerging use cases such as robotic perception, virtual reality (VR) applications, digital twins, and creating a 3D digital map of an environment. By identifying the material of surfaces and objects, robots can behave more intelligently during manipulation or handling of the objects, for example, by recognizing the objects' fragility robot can adjust the grip of the arm appropriately. VR systems can activate additional human senses (e.g., touch and smell) by using material information in a 3D digital map for emerging 6G use cases. For example, this supplemental material information can find applications in VR games, and emerging area of virtual tourism when travel disruption due to pandemic like COVID-19 is to arise.

Some of the existing material identification approaches rely on haptic recognition and spectroscopy methods. Haptic-recognition-based method requires direct contact with the object using haptic sensor and relies on pressing and sliding interactions of the sensor with the object to determine its material properties as shown in Fig. 1 [1]. In contrast to the haptic-recognition-based methods, spectroscopy-based methods do not require physical interaction between the object and the material detector but rely on interaction between object and electromagnetic radiation (as a function of the wavelength of the radiation) to recognize the material as shown in Fig. 2 [2]. In [2], material sensing of common objects such as

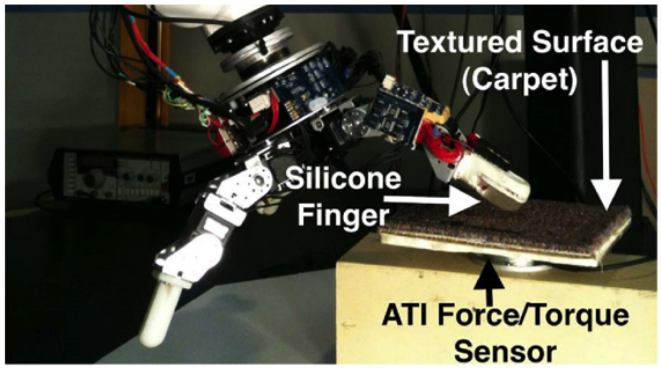

Fig. 1. Haptic-sensor-based material identification.

Fig. 2. Spectroscopy-based material identification.

wood, metal, plastic, paper, and fabric using spectroscopy was proposed. Here, authors proposed a neural network employing support vector machines (SVM) to separate the objects based on the spectrogram data. Materials and their properties can also be implied by analysing the structure of the molecules. This can be done by studying the vibrational modes and rotational frequencies. These are typically measured using time-domain spectroscopy (TDS). These methods require complex time-domain pulse generation equipment and sensors. In [3] authors proposed methods for drug property identification using terahertz (THz) TDS.

When it comes to using these methods in use cases such as robotic perception, VR applications, 3D mapping, and digital twins for material identification, haptic-sensor-based methods require a dedicated hardware and spectroscopy-based methods need object to be at least in centimeter level proximity to the detector for effective identification of the material. Therefore, both methods are not quite feasible when it comes to using them for realistic use cases where material detection plays a vital role.

To overcome the drawbacks of existing methods, in this paper, we propose a novel method that exploits radio signal that are typically transmitted in a wireless network for communication also for material identification. It is thus an example of joint communication and sensing (JCAS). Sensing here refers to information retrieved from received radio signals for objects to be identified in the environment surrounding the radio transceivers [4]. In 5G new radio (NR), reference signals such as demodulation reference signals (DMRS), channel state information reference signal (CSI-RS) in downlink and sounding reference signal (SRS) in uplink are used for channel estimation and can be optimized for the JCAS purpose [5], [6]. In [7], simulation results show that DMRS signal can be used as a primary signal for sensing and can provide decent accuracy. Apart from these reference signals, synchronization signal block (SSB) for cell search can be another candidate signal for JCAS. In general, it is evident that reference signals of 5G NR can be used for sensing [6].

Since its inception radio access technology (RAT) has been extensively used to provide seamless connectivity between communication devices for high capacity and secure communication by means of wireless radio signal transmission and reception. When a radio signal is transmitted between wireless transmitter and receiver devices, the radio signal is affected by the presence of multiple scatterers in and around the propagation path. The radio signal typically undergoes phenomena such as reflection, diffraction, and refraction depending on the type and nature of the obstacles it encounters while travelling from a transmitter to a receiver. These phenomena typically results into multi-path propagation of the radio signal, where the number and intensity of multi-path propagation depend heavily on the number of scatterers and their locations in the propagation path together with the radio signal waveform characteristics such as bandwidth and carrier frequency. Evaluating the strength of the signals that arrive at receiver via scatterers induced by multiple paths can therefore be used to establish an understanding of the type of scatterers that are located in and around the radio signal propagation environment. In this paper, we particularly propose a method that exploits the signals received at the receiver via a specular path to identify the material of the scatterer that are located in and around the radio signal propagation path. No additional hardware is needed for proposed method, material identification can be enabled on current wireless communication infrastructure. Furthermore, the object does not have to be in centimeter level proximity for effective material detection.

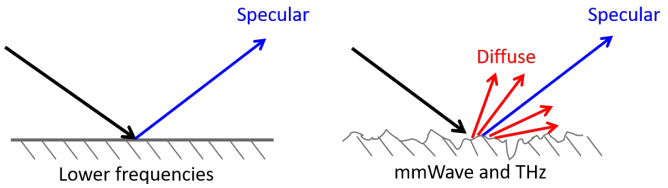

Fig. 3. Same surface exhibits different electrical roughness at different frequencies.

The common building surfaces like floors, exterior walls, windows, and ceilings are usually homogeneous and isotropic, and they tend to be electrically smooth at frequencies ranging up to mmWave because their surface height deviations are smaller than the radio signal wavelength [8]. At lower frequency bands (e.g., frequency range 1), diffuse scattering is negligible and the reflection propagation path is dominated, most energy is reflected to specular propagation path at a reflected angle that is equal to the incident angle [9]. However, in the frequency bands around and above mmWave bands (e.g., frequency range 2), the roughness of common building surfaces become electrically rough because the surface height deviations are comparable to the radio signal wavelength. Depending on the incident angle, there are substantial scattered signal paths. Different frequencies exhibit different intensity of specular and diffuse scattering from most building surfaces. Building surfaces appear electrically smooth at lower frequencies resulting in the specular reflections dominating the multi-paths, while same building surfaces induce both considerable diffuse scattering propagation paths and specular reflection path at mmWave and THz, as shown in Fig. 3 [9].

The Rayleigh roughness criterion is used to determine the roughness of a surface from electromagnetic point of view. The Rayleigh roughness criterion defines the standard height deviation h of a surface as [10]:

$$h = \frac{\lambda}{8 \cos \theta_i}, \tag{1}$$

where λ is the wavelength of a radio wave and θ_i is the incident angle. If a surface height deviation is smaller than standard height deviation h, the surface may be considered to be electrically smooth for the given frequency, otherwise the surface may be considered to be electrically rough for the given frequency [10].

TABLE I
PARAMETERS OF COMMON BUILDING MATERIALS

Material	Permittivity		Conductivity		Thickness (cm)	Roughness (mm)	Transparency
	a	b	c	d			
Plasterboard	2.94	0	0.0116	0.7076	5	0.2	0
Thick plasterboard	2.94	0	0.0116	0.7076	10	0.2	0
Glass	6.27	0	0.0043	1.1925	0.5	0	0.4
Heavy concrete	5.31	0	0.0326	0.8095	20	1	0
Medium concrete	5.31	0	0.0326	0.8095	10	1	0
Brick	3.75	0	0.038	0	20	2	0
Metal	1	0	1e7	0	1	0	0
Wood	1.99	0	0.0047	1.0718	10	0.3	0

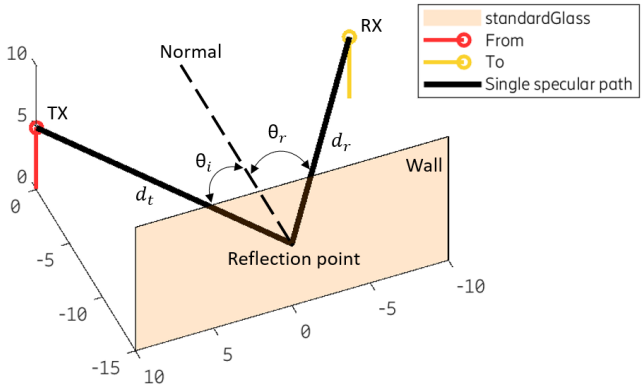

Fig. 4. Simulation setup - Step 1.

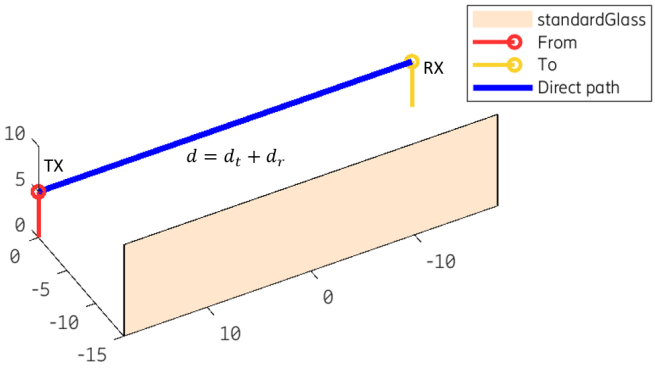

Fig. 5. Simulation setup - Step 2.

II. NUMERICAL VALIDATION

To study the contribution of reflection loss to estimate the materials of objects and surfaces, we did an extensive simulation based on Matlab. In this paper, we simulated narrow beam reflected by variety of common building materials namely: plasterboard, thick plasterboard, glass, heavy concrete, medium concrete, brick, metal, and wood with different incident angle θ_i at frequencies 2.6 GHz, 28 GHz, and 60 GHz. The parameters of materials in the simulation including permittivity, conductivity, and roughness recommended by ITU [11] are summarized in Table I. It is worth mentioning here that the roughness represents the root mean square value of the height deviation from perfectly smooth and higher value of roughness indicates less smooth surface of the material, lower value of transparency indicates that the object is opaque.

Two-step simulation was performed and the simulation setup is shown in Fig. 4 and Fig. 5, where a transmitter (TX) device and a receiver (RX) device (TX may refer to base station and RX may refer to terminal device in wireless communication system and vice versa) are placed in a free space scenario where the direct line of sight (LoS) path (blue line) between TX and RX is not blocked by any obstacle as shown in Fig. 5. By means of beam alignment, a highly directional vertically polarized signal is transmitted from TX, and a single-bounce reflection path between TX and RX is established, the signal reaches to RX via a specular reflection path (black line) after striking the wall at the reflection point as shown in Fig. 4. This paper assumes single-bounce-reflection path between TX and RX and does not consider multiple-bounce paths that have larger time of arrival (TOA) and weaker received signal strength (RSS) for the evaluation purpose [12]. Wall made up of materials listed in Table I is considered to generate a single-bounce path between TX and RX. The distance between TX/RX and wall is set to 15 m and TX/RX antenna heights are set to 5 m. The incident angle is maintained by changing the distance between TX and RX. For the simulation, incident angle θ_i with values 1.9°, 9.5°, 20.1°, 29.5°, 39.8°, 45°, 51.7°, 59°, 67.4°, 73.6°, and 81.6° are considered. A radio wave transmitted by TX incidents at an angle θ_i with respect to the normal of the wall surface as shown in Fig. 4. θ_r is reflected angle such that θ_i=θ_r, following Snell's law. d_t and d_r are the distances between the wall and the TX/RX, respectively. d is the overall propagation length of specular reflection path between TX/RX and $d = d_t + d_r$. To obtain reflection loss data, two-step simulation is performed. The first step is used to measure the amount of the received power reflected from surface of the wall with an incident angle θ_i determined by the TX/RX distance as shown in Fig. 4. The received power is the average power of transverse electric (TE) polarisation and transverse magnetic (TM) polarisation. The path loss (PL) over specular path is calculated as:

$$PL = P_{TX} - P_{RX}, \tag{2}$$

where P_{TX} is the transmitted power over specular path, P_{RX}

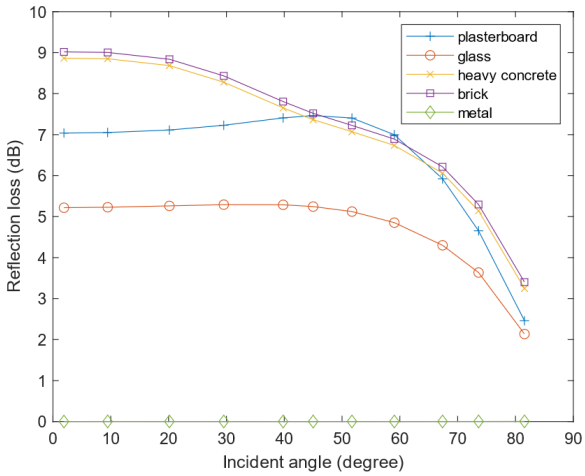

Fig. 6. Reflection losses of different materials at 2.6 GHz.

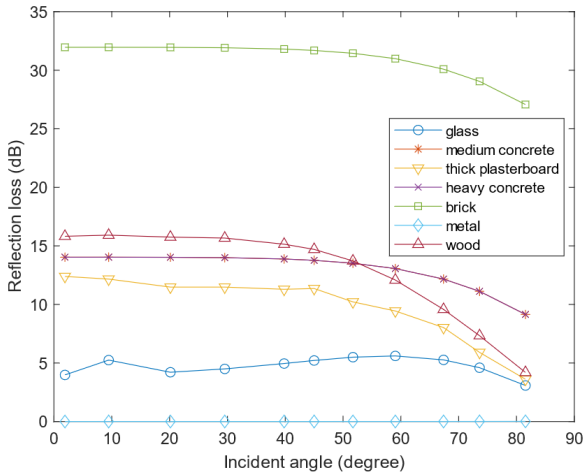

Fig. 7. Reflection losses of different materials at 28 GHz.

is the received power over specular path.

The second step constitutes a LoS transmission over the distance that is equal to d. From Friis' equation, the free space path loss ($FSPL$) over distance d is then calculated as:

$$FSPL(f,d) = 32.44 + 20\log_{10}(f) + 20\log_{10}(d), \quad (3)$$

where f is the carrier frequency in MHz and d is distance between TX and RX in kilometer.

Finally, the reflection loss (RL), which includes scattering loss and absorption loss, is calculated by subtracting (3) from (2) and is given by

$$RL = PL - FSPL(f,d), \quad (4)$$

It is worth noting that RL is independent of antenna type, antenna gain, transmitted power, and TX-RX distance. RL only corresponds to radio signal carrier frequency, scatterer properties, and the incident angle θ_i.

III. Results and Analysis

The simulation results of reflection losses of different materials at different incident angle θ_i at carrier frequencies 2.6 GHz, 28 GHz, and 60 GHz are reported in Fig. 6 to Fig. 8. It is evident that the reflection losses of different materials are different in most of the cases when incident angle θ_i is same for radio signals at carrier frequencies 2.6 GHz, 28 GHz, and 60 GHz. This clearly indicates that different materials can be effectively identified by using the radio signal and exploiting the reflection loss and incident angle information.

The simulation results show that as the frequency increases, the reflection loss increases, which can be expected according to (1), since the surfaces tend to be electrically rough (compared to the wavelength of the electromagnetic waves) as the frequency increases and rougher surfaces have higher tendency to scatter the radio signals. Take brick as an example, as shown in Fig. 9, brick (typical exterior surfaces of urban

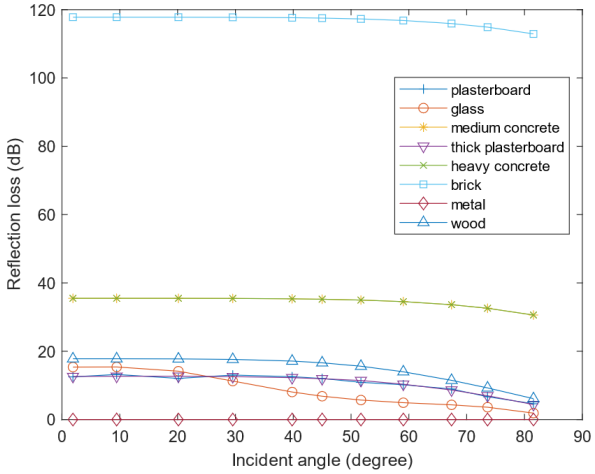

Fig. 8. Reflection losses of different materials at 60 GHz.

buildings) has reflection loss of less than 10 dB at 2.6 GHz, high reflection loss of approximately 30 dB and 115 dB at 28 GHz and 60 GHz, respectively. This illustrates the fact that bricky surface is electrically smooth at lower frequency but electrically rough at higher frequency, reflection losses of bricky surface are different at different frequencies, thus providing reflection loss isolation between multiple frequencies.

The rough brick has significantly different properties than the other materials. We can see from Fig. 9 that only at 2.6 GHz, brick has a significant reflected component. A rough bricky surface has very high reflection loss, more than 110 dB at 60 GHz, indicating that the effect of reflection loss from the rough surface is significantly larger than the reflection loss due to smoother materials.

Moreover, for all simulated frequencies, the reflection loss falls off when the incident angle θ_i increases. The minimum reflection loss is observed when the incident angle θ_i=81.6° (maximum θ_i was simulated). When the incident

TABLE II
REFLECTION LOSSES OF WOOD AND CONCRETE AT 28 GHZ AND 60 GHZ.

Material	**Reflection loss in dB at different incident angle (θ_i) in degree**										
	Carrier Frequency	1.9°	9.5°	20.1°	29.5°	39.8°	45°	51.7°	59°	67.4°	73.6°	81.6°
Wood	28 GHz	15.82	15.92	15.75	15.67	15.14	14.7	13.72	12.09	9.58	7.33	4.19
	60 GHz	17.79	17.79	17.76	17.62	17.12	16.62	15.62	13.99	11.49	9.27	6.12
Concrete	28 GHz	14.04	14.04	14.02	14	13.88	13.77	13.52	13.07	12.17	11.12	9.15
	60 GHz	35.5	35.5	35.49	35.46	35.34	35.23	34.98	34.52	33.63	32.58	30.6

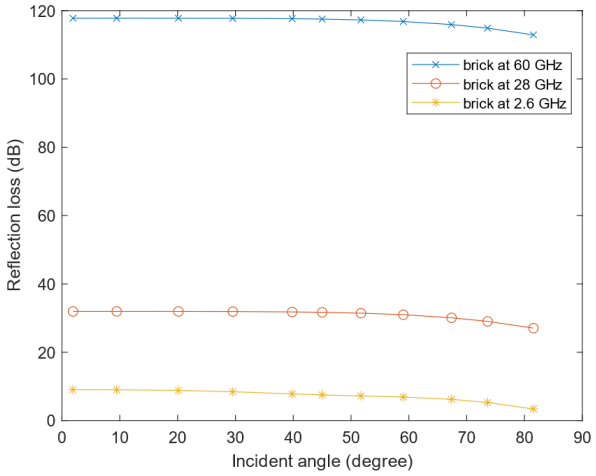

Fig. 9. Reflection losses of brick at 2.6 GHz, 28 GHz and 60 GHz.

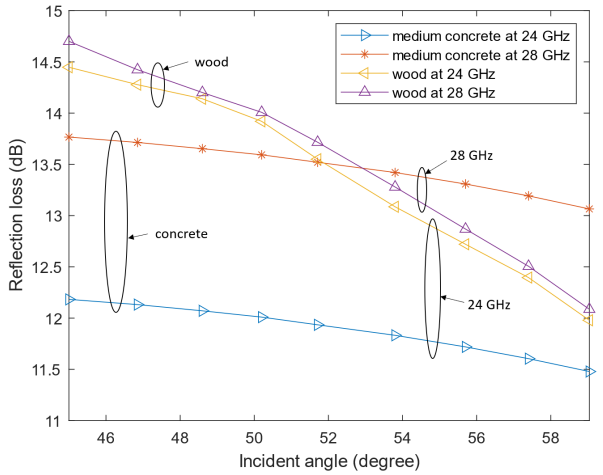

Fig. 10. Reflection loss of wood and concrete at 24 GHz and 28 GHz.

angle θ_i is large, the surface tends to be electrically smooth according to (1), therefore the scattering loss is low or negligible, then reflection loss (scattering loss plus absorption loss) is low, most of the energy is concentrated to specular reflection direction. However, when the incident angle is small (e.g., incident ray strikes the surface perpendicularly), the scattering loss is not negligible [9]. The scattered power is higher at small incident angles than at large incident angles. This is the reason why the reflection loss decreases when increasing the incident angle.

It is also observed from Fig. 6 to Fig. 8 that at 2.6 GHz, the reflection loss differences between most materials are quite small, especially when incident angle is large. For higher frequencies (28 GHz and 60 GHz), the reflection loss differences between most materials are pronounced, the curves are almost horizontal and most of them don't intersect each other when incident angle is small, which means the materials of the common building surfaces can be determined by reflection loss and approximate incident angle. When incident angle is large, reflection loss of materials declines with different rate, some reflection loss curves intersect with each other. Therefore, the materials of the common building surfaces can't be determined by reflection loss and approximate incident angle information at certain frequency. For example, Fig. 10 shows reflection losses of wood and concrete at 24 GHz and 28 GHz, including area where the reflection loss curves for wood and concrete intersect at incident angle 53° in Fig. 7. At incident angle 53°, wood and concrete induce similar reflection losses, thus the material of the surface can't be effectively determined by reflection loss and incident angle. In this type of situation, a multi-frequency evaluation is needed. For multi-frequency evaluation a radio signal at 24 GHz can be transmitted following the same propagation path taken by 28 GHz. When the carrier frequency of the radio signal changes, wood and concrete will induce different reflection losses at an incident angle of 53°. With significant difference in the reflection losses at 28 GHz and 24 GHz, the material of the surface can be effectively identified. It is worth noting here that the reflection loss induced by woody surface does not change much with the change in carrier frequency, but reflection loss induced by concrete surface changes significantly over different carrier frequency. The reflection loss difference for woody surface is found to be about 0.2 dB between 24 GHz and 28 GHz when incident angle is between 45° and 59° whereas the reflection loss difference for concrete surface is estimated to be around 1.58 dB.

The simulation result also shows that the material properties and incident angle are influencing factors of reflection loss rather than thickness when the thickness of material exceeds a certain value. For example, from Fig. 7, reflection loss curves of medium concrete (thickness 10 cm) and heavy concrete (thickness 20 cm) completely overlap with each other. Furthermore, it is worth noting that the simulation results

reported in figures from Fig. 6 to Fig. 8 verify that smoother surface (metal and glass) induce lower reflection loss.

IV. REFLECTION-LOSS-BASED MATERIAL IDENTIFICATION METHOD

Based on the simulation results, a reflection-loss-based material identification method for fast material identification in a multi-path wireless communication environment was developed. The core idea is to identify the material based on comparing measured reflection loss of an electromagnetic signal from its surface with pre-recorded reflection losses from different materials stored in a database. The proposed method comprises of the following steps:

- Step 1: Measuring or simulating the reflection losses from different materials at different frequency/frequencies and incident angle/angles to create a database.
- Step 2: Transmitting radio signal via beams at certain frequency/frequencies towards the material from a transmitter at certain angle/angles and measuring reflection loss based on the received signal at a receiver.
- Step 3: Comparing the measured reflection loss with pre-measured reflection losses from different materials that are recorded in a database to identify the material.

In Step 1, a reflection loss lookup database for different materials is pre-measured or pre-simulated. The lookup database is an array including materials, frequencies, incident angles and reflection losses information, such that runtime material identification procedure is reduced by implementing a simpler array indexing operation. Pre-measurement is the act of performing an initial reflection loss measurement to generate a lookup database that can be used by proposed material identification method to avoid repeated computation every time when material identification needs to be done. The reflection losses of multiple incident angles are measured by changing the distance between TX and RX as shown in Fig. 4.

An example lookup database based on pre-simulation is shown in Table II. For simplicity, only reflection losses of wood and concrete at 28 GHz and 60 GHz are listed with 11 different incident angles.

In Step 2 and 3, by means of beam sweeping, a beam pair is established between TX and RX, and the non-LoS (NLoS) beam is single-bounce-reflected by an object to be identified. The material identification processing unit calculates the reflection loss according to transmitted power, received power, incident angle and frequency. For example if one of the measurement sets, where reflection loss of 14 dB is measured at θ_i=40° and f=28 GHz, the material inducing this reflection loss can be identified as concrete by database look up operation where reflection loss of 13.88 dB is pre-measured for 28 GHz radio signal when the incident angle is 39.8°. Moreover, the reflection point can be localized by determining the intersection point of transmitter-side beam and receiver-side beam lie on a co-plane. Therefore, a data point including its coordinate (x,y,z) and material information is obtained. By collecting enough data points in an environment, a 3D digital map with material information can be generated.

V. CONCLUSIONS

In this paper a novel material identification method based on joint communication and sensing is proposed. The proposed method does not require additional hardware but by what is anyway deployed for wireless communication purposes and relies on reflection loss evaluation of radio signal induced by the material type of the object that is encountered while the radio signal propagates from a transmission point to a reception point in a typical wireless communication network. The proposed method uses a simple array indexing approach for material identification and bears significantly less computational burden in comparison to a parametric-model-based approach. The proposed method can be effectively integrated to future RAT systems to generate 3D digital maps with material information and support new and emerging use cases where effective material identification plays a vital role.

ACKNOWLEDGMENT

This work has been partly funded by the European Commission through the H2020 project Hexa-X (Grant Agreement no. 101015956).

REFERENCES

[1] N. Jamali and C. Sammut, "Majority Voting: Material Classification by Tactile Sensing Using Surface Texture," in IEEE Transactions on Robotics, vol. 27, no. 3, pp. 508-521, June 2011.

[2] Z. Erickson, N. Luskey, S. Chernova and C. C. Kemp, "Classification of Household Materials via Spectroscopy," in IEEE Robotics and Automation Letters, vol. 4, no. 2, pp. 700-707, April 2019.

[3] E. García-García, E. Diez, Y. M. Meziani, J. E. Velázquez-Pérez and J. Calvo-Gallcao, "Terahertz time domain spectroscopy for chemical identification," 2013 Spanish Conference on Electron Devices, Valladolid, 2013, pp. 199-202.

[4] M. L. Rahman, J. A. Zhang, X. Huang, Y. J. Guo and R. W. Heath, "Framework for a Perceptive Mobile Network Using Joint Communication and Radar Sensing," in IEEE Transactions on Aerospace and Electronic Systems, vol. 56, no. 3, pp. 1926-1941, June 2020.

[5] 3GPP TS 38.211, "Physical channels and modulation," V16.3.0, September 2020.

[6] M. L. Rahman et al., "Enabling Joint Communication and Radio Sensing in Mobile Networks – A Survey," https://arxiv.org/abs/2006.07559v2.

[7] M. L. Rahman, P. Cui, J. A. Zhang, X. Huang, Y. J. Guo and Z. Lu, "Joint Communication and Radar Sensing in 5G Mobile Network by Compressive Sensing," 2019 19th International Symposium on Communications and Information Technologies (ISCIT), Ho Chi Minh City, Vietnam, 2019, pp. 599-604.

[8] A. A. Goulianos et al., "Measurements and Characterisation of Surface Scattering at 60 GHz," 2017 IEEE 86th Vehicular Technology Conference (VTC-Fall), Toronto, ON, 2017, pp. 1-5.

[9] T. S. Rappaport et al., "Wireless Communications and Applications Above 100 GHz: Opportunities and Challenges for 6G and Beyond," in IEEE Access, vol. 7, pp. 78729-78757, 2019.

[10] T. S. Rappaport, Wireless Communications: Principles and Practice, 2nd ed. Upper Saddle River, NJ: Prentice Hall, 2002.

[11] Effects of building materials and structures on radiowave propagation above about 100 MHz, International Telecommunications Union Recommendation ITU-R P.2040-1, July 2015.

[12] K. Han, S. Ko, H. Chae, B. Kim and K. Huang, "Hidden Vehicle Sensing via Asynchronous V2V Transmission: A Multi-Path-Geometry Approach," in IEEE Access, vol. 7, pp. 169399-169416, 2019.